Accepted Manuscript of: Abdelrahman, Y., Khuri, S.A. & Louhichi, I. A numerical investigation of the buckling of a doubly clamped nano-actuators governed by an integro-differential equation. *Journal of Mathematical Sciences* (2022).
This version of the article has been accepted for publication after peer review and is subject to Springer Nature's AM terms of use, but is not the Version of Record and does not reflect post-acceptance improvements, or any corrections. The Version of Record is available at: https://doi.org/10.1007/s10958-022-05886-w

A NUMERICAL INVESTIGATION OF THE BUCKLING OF DOUBLY CLAMPED NANO-ACTUATORS GOVERNED BY AN INTEGRO-DIFFERENTIAL EQUATION

YOUSSEF ABDELRAHMAN [1,2], SUHEIL A. KHURI [2], AND ISSAM LOUHICHI [3,*]

Abstract. In this article, a fixed point iterative scheme involving Green's function is applied to reach a solution for the buckling of nano-actuators under nonlinear forces. Our solution is convergent. The nano-actuators problem under consideration is governed by a general type equation that contains nonlinear forces and integro-differential terms. The equation, we adopted and which governs the nano-actuators, is a nonlinear integro-differential BVP of fourth order. Our scheme enjoys important features such as high accuracy, robustness, and fast convergence. Numerical tests are performed and compared with other results that exist in the current literature.

1. Introduction

In recent years, a wide spectrum of articles have been devoted to investigate the buckling of doubly clamped nano-actuators with an integro-differential governing equation. Ansari *et al.* [2] and Bacciocchi *et al.* [3] applied the Generalized Differential Quadrature (GDQ) method to numerically solve the governing equations of nanoplates. The governing equations were discretized along with simply-supported and clamped boundary conditions using the GDQ method which was proven to be an accurate, stable and reliable numerical tool. In contrast, Shanab *et al.* [25] implemented the Generalized Differential Quadrature technique to discretize the nonlinear nonclassical governing differential equations and the nonclassical boundary conditions, and then used the Hamilton's principle to obtain nonclassical boundary conditions. SoltanRezaee *et al.* [27] applied the Hamiltonian principle to derive the nonlinear governing equations of nano-cantilevers. After validation of their results by previous available numerical results, the pull-in voltages and fundamental natural frequencies of the actuated nano-beam were achieved numerically using the Step-by-Step Linearization Method. Mohebshashedin and Farrokhabadi used two different numerical approaches to solve the differential governing equation, namely Runge Kutta Method (RKM) and an approximated Reduced Order Method (ROM) [20]. Quite a few papers (see [7], [18], [19], [24], [28], and [30]) used the modified Adomian Decomposition Method (MADM) to obtain an analytical solution for the bucking and pull-in instability of the actuator. The MADM's semi–analytical series solutions were compared with the existing numerical ones and they were found to be compatible and in good agreement . Younis *et al.* [31] presented an analytical approach and a reduced-order model (macromodel) to investigate the behavior of electrically actuated microbeam-based MEMS. Ghalambaz *et al.* [8] utilized a power series solution to study the deflection and pull–in instability of nano-cantilever electromechanical switches using a distributed parameter model, while Noghrehabadi *et al.* [23] used a power series solution to study

the effect of intermolecular forces on the instability of multi walled carbon nanotube (MWCNT) probes/actuators in the vicinity of thin and thick graphite. In [26], Shivanian and Ansari transform the governing equation into an equivalent problem whose boundary conditions are homogeneous in the internal $[-1, 1]$, and then use optimized Chebyshev polynomials to construct approximate series solution with unknown weights. Other techniques have been also employed for the differential governing equations: those methods include but not limited to Variational Iteration Method (VIM) [11], Homotopy Perturbation Method (HPM) [22], Adomian Decomposition Method and Padé approximants [24], Monotone Positive Method [21], and Rayleigh-Ritz Method [12]. Alternative strategies that can be exploited to tackle our investigated problem as well as other engineering models can be found in [15], [16], [29], [5], [6], and the references therein.

Some applications of the differential governing equations arise in many scientific and engineering applications including physical oceanography, in the framework of heat conduction, multi-layer beam, the deflection of a curved beam with a constant or varying cross-section, , the theory of variational inequality , the rocket's motion, thin liquid film, aerospace engineering, civil engineering, mechanical engineering, naval engineering, chemical engineering, biomedical implants, energy, defense, optoelectronics, bio-engineering, medicine, electronics, nano-scale fabrications, sensing, mass-detecting, underground water flow, thermoelasticity, plasma physics, electromagnetic waves, gravity-driven flows, the study of boundary layer theory, draining and coating flows, stellar interiors, control and optimization theory and flow networks in biology and in many branches of pure and applied mathematics (see [4] and [12] and the references therein).

The ultimate goal of this study is to implement a newly developed method (see [1], [9], [10], [13], [14], [17] and the references therein) for the solution of the equation that governs clamped-clamped nano-actuators, in which the latter are obeying nonlinear forces. Such forces could be applied voltage, electrostatic forces, the fringing field effect, the Casimir effect, the capillary effect and the dielectric layer effect. Furthermore, the nonlinear integral term in our equation that governs nano-actuators is due to the existence of axial loads. The method is an iterative scheme based on applying well-known fixed point iterative procedures, e.g., Picard's and Mann's iterative schemes, to some linear integral operator. This linear operator involves the Green's function of the linear differential term in the model equation. In this article, we consider a governing equation of general form that includes an integro-differential component. The proposed method is utilized to obtain highly accurate solution of the buckling of nano-actuators and to overcome the shortcomings of other methods, particularly the deterioration of the error as we move away from the initial left endpoint of the interval or as the domain becomes large. As a case study, we compared our results with the results of other numerical methods that exist in the literature. Our solution produces relations that describe how the nano-actuator depends on the free-dimensional parameters. These relations are useful in the conception of nano-actuators.

The manuscript is arranged as follows. In Section 2, we present the mathematical model under investigation. In section 3, we give an overview of the construction of the

Green's function, then present and describe the fixed point iterative method. Section 4 is devoted to a numerical case study to confirm and illustrate the convergence of our method. The concluding remarks are reported in Section 5 in which we summarize the numerical outcomes.

2. Our model

Under the presence of nonlinear forces and axial loads, we consider the following free-dimensional equation that governs a nano-actuator beam [7]

$$\frac{d^4u}{dx^4} - \left(\eta \int_0^1 \left(\frac{du}{dx}\right)^2 dx + P\right) \frac{d^2u}{dx^2} = -\frac{\alpha}{u^\zeta} - \frac{\beta}{(\kappa+u)^2} - \frac{\gamma}{u}. \tag{2.1}$$

In the case of the clamped-clamped nano-actuators, this equation satisfies the boundary conditions (BCs)

$$u(0) = 1, \quad u(1) = 1, \quad u'(0) = 0, \quad u'(1) = 0. \tag{2.2}$$

Here the independent variable x is the length of the beam and the dependent variable u is its deflection. The free-dimensional parameters η, P, β, γ and κ are such that: P and η denote the axial loads, β is the voltage applied externally, κ is the dielectric layer force, and γ represents the capillary action or the force due to fringing field. Finally, ζ is a natural number. In the case of $\zeta = 3$, the free-dimensional parameter α denotes the effects of van der Waals, and when $\zeta = 4$, α denotes the Casimir force.

3. Illustration of the Iterative method

In what follows we describe the proposed fixed point iterative scheme that is expressed using the Green's function of the linear term in (2.1).

3.1. **Green's Function.**

First, we shall explain how to obtain the Green's function for a class of linear 4^{th} order BVPs. We start with the following linear equation

$$L[u] = u^{(4)}(x) + s_1(x)u^{(3)}(x) + s_2(x)u''(x) + s_3(x)u'(x) + s_4(x)u(x) = f(x), \tag{3.3}$$

for $0 \leq x \leq 1$, and with the boundary conditions

$$u(0) = l_1, \quad u'(0) = l_2, \quad u(1) = l_3, \quad u'(1) = l_4. \tag{3.4}$$

The general solution of (3.3)-(3.4) is given by $u = u_h + u_p$, where u_h satisfies the homogeneous equation $L[u] = 0$ with BCs (3.4), and u_p is a particular solution to $L[u] = f(x)$ subject to the corresponding homogeneous BCs

$$u(0) = u'(0) = u(1) = u'(1) = 0. \tag{3.5}$$

In order to find a particular solution u_p, we compute the Green's function $G(x, s)$ which satisfies the equation

$$-L[u] = \delta(x - s), \tag{3.6}$$

subject to the BCs (3.5). Then, u_p is given by

$$u_p = \int_0^1 G(x,s) f(s)\, ds. \tag{3.7}$$

When $x \neq s$, $G(x,s)$ satisfies $L[u] = 0$. Hence, $G(x,s)$ can be written as

$$G(x,s) = \begin{cases} a_1u_1 + a_2u_2 + a_3u_3 + a_4u_4 & 0 \leq s \leq x \leq 1 \\ b_1u_1 + b_2u_2 + b_3u_3 + b_4u_4 & 0 \leq x \leq s \leq 1 \end{cases},$$

where u_1, u_2, u_3 and u_4 are solutions to $L[u] = 0$ and linearly independent. The values of the constants $a_1, a_2, a_3, a_4, b_1, b_2, b_3, b_4$ are determined as follows:

1. G satisfies the four BCs (3.5).
2. G is continuous at $s = x$:

$$a_1u_1(x) + a_2u_2(x) + a_3u_3(x) + a_4u_4(x) = b_1u_1(x) + b_2u_2(x) + b_3u_3(x) + b_4u_4(x).$$

3. G' is continuous at $s = x$:

$$a_1u_1'(x) + a_2u_2'(x) + a_3u_3'(x) + a_4u_4'(x) = b_1u_1'(x) + b_2u_2'(x) + b_3u_3'(x) + b_4u_4'(x).$$

4. G'' is continuous at $s = x$:

$$a_1u_1''(x) + a_2u_2''(x) + a_3u_3''(x) + a_4u_4''(x) = b_1u_1''(x) + b_2u_2''(x) + b_3u_3''(x) + b_4u_4''(x).$$

5. $G^{(3)}$ has a unit jump discontinuity at $s = x$:

$$b_1u_1^{(3)}(x)+b_2u_2^{(3)}(x)+b_3u_3^{(3)}(x)+b_4u_4^{(3)}(x)-a_1u_1^{(3)}(x)-a_2u_2^{(3)}(x)-a_3u_3^{(3)}(x)-a_4u_4^{(3)}(x) = -1.$$

For a nonlinear 4^{th} order BVP

$$u^{(4)} + p(x)u^{(3)} + q(x)u'' + r(x)u' + s(x)u = f\left(x, u, u', u'', u^{(3)}\right), \tag{3.8}$$

a particular solution, subject to the BCs (3.5), is given by

$$u_p = \int_0^1 G(x,s)\, f\left(s, u_p, u_p', u_p'', u_p^{(3)}\right)\, ds. \tag{3.9}$$

For the sake of completeness, we evaluate the Green's function for the following family of BVPs:

$$\begin{cases} u^{(4)} = f\left(x, u, u', u'', u^{(3)}\right), \\ u(0) = u(1) = 2, u'(0) = -1, u'(1) = 5. \end{cases} \tag{3.10}$$

Observe that the general solution of the associated homogeneous equation $u^{(4)}(x) = 0$ is $u_h = ax^3 + bx^2 + cx + d$. The Green's function is given by

$$G(x,s) = \begin{cases} a_1s^3 + b_1s^2 + c_1s + d_1, & 0 \leq s \leq x \leq 1 \\ a_2s^3 + b_2s^2 + c_2s + d_2, & 0 \leq x \leq s \leq 1 \end{cases}. \tag{3.11}$$

The previous five conditions yield:

$$
\begin{cases}
d_1 = 0, \\
a_2 + b_2 + c_2 + d_2 = 0, \\
c_1 = 0, \\
3a_2 + 2b_2 + c_2 = 0, \\
a_1x^3 + b_1x^2 + c_1x + d_1 = a_2x^3 + b_2x^2 + c_2x + d_2, \\
3a_1x^2 + 2b_1x + c_1 = 3a_2x^2 + 2b_2x + c_2, \\
6a_1x + 2b_1 = 6a_2x + 2b_2, \\
6a_2 - 6a_1 = -1.
\end{cases} \tag{3.12}
$$

After solving this linear system, we obtain that

$$
G(x,s) = \begin{cases}
\left(\frac{1}{3}x^3 - \frac{1}{2}x^2 + \frac{1}{6}\right)s^3 - \left(\frac{1}{2}x^3 - x^2 + \frac{1}{2}x\right)s^2, & 0 \le s \le x \le 1 \\
\left(\frac{1}{3}x^3 - \frac{1}{2}x^2\right)s^3 - \left(\frac{1}{2}x^3 - x^2\right)s^2 - \frac{1}{2}x^2s + \frac{1}{6}x^3, & 0 \le x \le s \le 1
\end{cases} \tag{3.13}
$$

3.2. **Picard-Green's Scheme (PGS).** In this subsection, we describe our proposed method. We consider the following family of 4^{th} order BVPs

$$
L[u] \equiv u^{(4)} + a_1(x)u^{(3)} + a_2(x)u'' + a_3(x)u' + a_4(x)u = f\left(x, u, u', u'', u^{(3)}\right) \tag{3.14}
$$

with the BCs (3.4). We then define the integral operator

$$
K[u] = \int_0^1 G(x,s)L[u]\,ds, \tag{3.15}
$$

G is the Green's function for the corresponding $L[u] = 0$. Observe that u is a fixed point of K if and only if u is a solution of (3.14). By adding and subtracting f from the integrand, we have

$$
\begin{aligned}
K[u] &= \int_0^1 G(x,s)\left[L[u] - f\left(s, u(s), u'(s), u''(s), u^{(3)}(s)\right)\right]\,ds \\
&+ \int_0^1 G(x,s)\,f\left(s, u(s), u'(s), u''(s), u^{(3)}(s)\right)\,ds.
\end{aligned} \tag{3.16}
$$

Using (3.9), equation (3.16) implies

$$
K[u_p] = \int_a^b G(x,s)\left[L[u_p] - f\left(s, u_p(s), u_p'(s), u_p''(s), u_p^{(3)}(s)\right)\right]\,ds + u_p, \tag{3.17}
$$

where u_p is a particular solution. At this stage, we apply Picard's iterative scheme which is

$$
u_{n+1} = K[u_n], \quad n = 0, 1, \ldots
$$

on the operator in (3.17). This results in the following iterative scheme, which we will refer to by PGS

$$
u_{n+1} = u_n + \int_a^b G(x,s)\left[L[u_n] - f\left(s, u_n(s), u_n'(s), u_n''(s), u_n^{(3)}(s)\right)\right]\,ds. \tag{3.18}
$$

Here u_p is replaced by u for convenience.

Remark 1. *If we apply instead of Picard's Mann's fixed point iterative scheme on $K[u]$ i.e.*

$$u_{n+1} = (1-\alpha_n)u_n + \alpha_n K[u_n], \qquad \forall n \geq 0, \tag{3.19}$$

where α_n is a sequence in $[0,1]$, then by simple calculations, we obtain the following iterative scheme, which we denote by MGS

$$u_{n+1} = u_n + \alpha_n \int_a^b G(x,s)\left[L[u_n] - f\left(s, u_n(s), u_n'(s), u_n''(s), u_n^{(3)}(s)\right)\right] ds. \tag{3.20}$$

In general, Mann's iterative scheme has the advantage of overcoming divergence of Picard's scheme. In fact, it can speed the rate of convergence when the sequence α_n is carefully chosen. Observe that when $\alpha_n = 1$, Mann's becomes Picard's. For both PGS and MGS, the initial point u_0, is chosen to satisfy $L[u] = 0$ with the BCs in (3.4). Moreover, to find the optimal values of α_n that assure the fastest rate of convergence, we minimize the $L^2[a,b]$-norm of the residual error, $R_n(x;\alpha_n)$, of the n^{th} iteration u_n, e.g., if u_1 is the first iterate, we minimize for α_1 the corresponding L^2-norm of the residual error $R_1(x;\alpha_1)$, which is given by

$$\|R_1(x;\alpha_1)\|_{L^2}^2 \;=\; \int_a^b |R_1(x;\alpha_1)|^2 dx.$$

The other values of α_n are obtained in a similar way. Nevertheless, for the equations in study and when running our numerical codes, it turns out for us that the best α_n is 1. This is why we shall stick to PGS from now on.

4. Convergence Analysis

Without loss of generality, we consider the following 4^{th} order nonlinear BVP

$$u^{(4)}(x) = f(x, u, u', u'', u^{(3)}), \text{ for } 0 < x < 1,$$

subject to

$$u(0) = u(1) = 1 \text{ and } u'(0) = u'(1) = 0.$$

Then the Green's function is

$$G(x,s) = \begin{cases} (\frac{1}{3}x^3 - \frac{1}{2}x^2 + \frac{1}{6})s^3 - (\frac{1}{2}x^3 - x^2 + \frac{1}{2}x)s^2, & 0 \leq s \leq x \leq 1 \\ (\frac{1}{3}x^3 - \frac{1}{2}x^2)s^3 - (\frac{1}{2}x^3 - x^2)s^2 - \frac{1}{2}x^2 s + \frac{1}{6}x^3, & 0 \leq x \leq s \leq 1 \end{cases}$$

and the Picard-Green's iterative scheme is given by

$$u_{n+1} \;=\; u_n + \int_0^1 \left[G(x,s)u^{(4)}(s) - G(x,s)f(s,u,u',u'',u^{(3)})\right] ds. \tag{4.21}$$

Because $G(x,0) = G(x,1) = \frac{\partial G}{\partial s}(x,0) = \frac{\partial G}{\partial s}(x,1) = 0$, $-L(G(x,s)) = \delta(x-s)$, and using integration by parts four times, we obtain

$$\begin{aligned}
\int_0^1 G(x,s)u^{(4)}(s)ds &= G(x,s)u^{(3)}(s)\big|_0^1 - \int_0^1 G'(x,s)u^{(3)}(s)ds \\
&= -\frac{\partial G}{\partial s}(x,s)u''(s)\Big|_0^1 + \int_0^1 \frac{\partial^2 G}{\partial s^2}(x,s)u''(s)ds \\
&= \frac{\partial^2 G}{\partial s^2}(x,1)u'(1) - \frac{\partial^2 G}{\partial s^2}(x,0)u'(0) - \int_0^1 \frac{\partial^3 G}{\partial s^3}(x,s)u'(s)ds \\
&= \frac{\partial^3 G}{\partial s^3}(x,1)u'(1) - \frac{\partial^3 G}{\partial s^3}(x,0)u'(0) + \int_0^1 \frac{\partial^4 G}{\partial s^4}(x,s)u(s)ds \\
&= (3x^2 - 2x^3) + (2x^3 - 3x^2 + 1) - \int_0^1 \delta(x-s)u(s)\,ds \\
&= 1 - u(x).
\end{aligned}$$

We then define the linear operator K_G, from $\mathcal{C}^4([0,1])$ into itself, by

$$K_G(u)(x) = u(x) + \int_0^1 \left[G(x,s)u^{(4)}(s) - G(x,s)f(s,u,u',u'',u^{(3)})\right]\,ds.$$

Thus the iterative scheme (4.21) becomes

$$u_{n+1} = K_G(u_n). \tag{4.22}$$

We shall show that, under some hypothesis on the function f, the operator K_G is a contraction on the Banach space $\mathcal{C}^4([0,1])$ with respect to the norm $||u||_{\mathcal{C}^4} = \sum_{k=0}^3 \sup_{[0,1]} |u^{(k)}(x)|$, and therefore the sequence (u_n) defined by (4.22) with $u_0(x) = 1$ converges strongly to the fixed point of K_G.

Theorem 1. *Assume that the function f, in the expression of the operator K_G, satisfies a Lipschitz condition of the form*

$$|f(x,u,u',u'',u^{(3)}) - f(x,v,v',v'',v^{(3)})| \leq \sum_{k=0}^{3} L_k |u^{(k)}(x) - v^{(k)}(x)|,$$

where the L_k's are positive constants such that

$$\frac{1}{192} \max_{0\leq k\leq 3}\{L_k\} < 1.$$

Then the operator K_G is a contraction on the Banach space $(\mathcal{C}^4([0,1]), ||.||_{\mathcal{C}^4})$, and hence the Picard-Green's iteration $(u_n)_n$ of (4.21) converges strongly to the fixed point of K_G.

Proof.

$$\begin{aligned}
|K_G(u)(t) - K_G(v)(t)| &= \Big|u(x) + \int_0^1 G(x,s)\left[u^{(4)}(s) - f(s,u,u',u'',u^{(3)})\right]\, ds \\
&- v(x) - \int_0^1 G(x,s)\left[v^{(4)}(s) - f(s,v,v',v'',v^{(3)})\right]\, ds\Big| \\
&= \left|\int_0^1 G(x,s)\left[f(s,v,v',v'',v^{(3)}) - f(s,u,u',u'',u^{(3)})\right]\, ds\right| \\
&\leq \int_0^1 |G(x,s)|\left|f(s,v,v',v'',v^{(3)}) - f(s,u,u',u'',u^{(3)})\right|\, ds \\
&\leq \sup_{[0,1]\times[0,1]} |G(x,s)| \int_0^1 \left|f(s,v,v',v'',v^{(3)}) - f(s,u,u',u'',u^{(3)})\right|\, ds \\
&= G(\frac{1}{2},\frac{1}{2}) \int_0^1 \left|f(s,v,v',v'',v^{(3)}) - f(s,u,u',u'',u^{(3)})\right|\, ds \\
&= \frac{1}{192}\int_0^1 \left|f(s,v,v',v'',v^{(3)}) - f(s,u,u',u'',u^{(3)})\right|\, ds \\
&\leq \frac{1}{192}\int_0^1 \left(\sum_{k=0}^{3} L_k |v^{(k)}(s) - u^{(k)}(s)|\right)\, ds \\
&\leq \frac{1}{192}\max_{0\leq k\leq 3}\{L_k\}\int_0^1 \left(\sum_{k=0}^{3} |v^{(k)}(s) - u^{(k)}(s)|\right)\, ds \\
&\leq \frac{1}{192}\max_{0\leq k\leq 3}\{L_k\}\sum_{k=0}^{3}\sup_{[0,1]} |v^{(k)}(s) - u^{(k)}(s)| \\
&< ||u-v||_{\mathcal{C}^4}.
\end{aligned}$$

□

5. Numerical Results

In this section, we present our numerical results for some case studies as have been adopted in [7] and [30].

In [30], the authors analyzed how a nano-actuator behaves when there is a layer of water beneath of it. For this case, the equation which governs of the nano-actuator is given by

$$\frac{d^4u}{dx^4} - \left(\eta\int_0^1 \left(\frac{du}{dx}\right)^2 dx\right)\frac{d^2u}{dx^2} = -\frac{\alpha}{u^4} - \frac{\beta}{(\kappa+u)^2} - \frac{\gamma}{u},$$

with $\alpha, \beta, \gamma, \eta$ and κ being the free-dimensional parameters of Casmir effect, externally applied voltage, the force due to fringing field , the axial loads, and the dielectric layer effect, respectively. Note $P = 0$ which means that the effect of its axial load is neglected. In this study, we use our proposed PGS (3.18) to solve this problem numerically, in the

typical case when $P = 0$. In this case, the iterative scheme (3.18) is given by:

$$\begin{aligned} u_{n+1}(x) &= u_n(x) + \int_0^x \left[\left(\frac{1}{3}x^3 - \frac{1}{2}x^2 + \frac{1}{6}\right)s^3 - \left(\frac{1}{2}x^3 - x^2 + \frac{1}{2}x\right)s^2\right] \\ &\quad \left[u_n^{(4)}(s) - \left(\eta\int_0^1 (u_n'(s))^2\,ds\right)u_n''(s) + \frac{\alpha}{u_n^4(s)} + \frac{\beta}{(\kappa + u_n(s))^2} + \frac{\gamma}{u_n(s)}\right] ds \\ &+ \int_x^1 \left[\left(\frac{1}{3}x^3 - \frac{1}{2}x^2\right)s^3 - \left(\frac{1}{2}x^3 - x^2\right)s^2 - \frac{1}{2}x^2 s + \frac{1}{6}x^3\right] \\ &\quad \left[u_n^{(4)}(s) - \left(\eta\int_0^1 (u_n'(s))^2\,ds\right)u_n''(s) + \frac{\alpha}{u_n^4(s)} + \frac{\beta}{(\kappa + u_n(s))^2} + \frac{\gamma}{u_n(s)}\right] ds, \end{aligned} \tag{5.23}$$

where, according to Remark 1, u_0 is the solution to the homogeneous equation

$$L[u] = u^{(4)}(x) = 0$$

subject to the BCs (2.2), namely $u(0) = u(1) = 1$ and $u'(0) = u'(1) = 1$. This yields $u_0(x) = 1$.

To execute this iterative scheme, we use the Computer Algebra System *Maple*. The transition from one iteration to the next is done symbolically and numerically. The latter occurs when approximating the integral appearing in (5.23) using Taylor polynomials. As far as the CPU time is concerned, it was not an issue for us since *Maple* takes only a few seconds to execute the iterations. To validate our results, we compute the residual errors. The values reported in Table 2, Table 5, and Table 7 show that our numerical solution satisfies the governing integro-differential equation with high accuracy within only a few iterations. Moreover, Figure 1 is compatible with the result obtained in [26].

As a consequence of the symmetry of the beam, the maximum of the deflection occurs when $x = 0.5$. At rest and when there are no applied forces, the shape of the beam is a straight segment line and can be modeled as $u(x) = 1$. When forces are applied, the beams deflects from its positions at rest and this deflection can then be expressed by the term $1-u(x)$. Table 1, Table 4, and Table 6 present numerical values of $1-u(0.5)$, namely the largest deflection of the beam for different values of α, β, ξ, γ, κ, and η. Observe that, with 40 iterations, we obtain the maximum deflection accurate to 12 decimal places. A comparison of the maximum deflection value obtained by our method versus those found in Yazdanpanahi *et al.* [30] and Ghalambaz *et al.* [7] is reported in Table 3.

TABLE 1. Largest deflection of a nano-actuator with $\alpha = 20$, $\beta = 5$, $\xi = 4$, $\gamma = 0.325$, $P = 0$, $\kappa = -0.396$, and $\eta = 0.96$.

Number of iterations	Maximum deflection of a nano-actuator
$n = 4$	0.131633936442778092193918 0
$n = 8$	0.135351491059452886988690 4
$n = 12$	0.135518672724204485678702 8
$n = 16$	0.135526310858968578070927 7
$n = 20$	0.135526660066952892464686 7
$n = 24$	0.135526676032896528594503 5
$n = 28$	0.135526676762867583002460 0
$n = 32$	0.135526676796242232646521 4
$n = 36$	0.135526676797768138688227 4
$n = 40$	0.135526676797837903892454 7

TABLE 2. Residual errors for the case $\alpha = 20$, $\beta = 5$, $\xi = 4$, $\gamma = 0.325$, $P = 0$, $\kappa = -0.396$, and $\eta = 0.96$.

x	$n = 4$	$n = 8$	$n = 12$	$n = 16$	$n = 20$	$n = 24$	$n = 28$	$n = 32$	$n = 36$	$n = 40$
0.1	9.15(−2)	4.04(−3)	1.85(−4)	8.43(−6)	3.86(−7)	1.76(−8)	8.06(−10)	3.69(−11)	1.71(−12)	9.82(−14)
0.2	3.00(−1)	1.32(−2)	6.01(−4)	2.75(−5)	1.26(−6)	5.75(−8)	2.63(−9)	1.20(−10)	5.49(−12)	2.51(−13)
0.3	6.45(−1)	2.86(−2)	1.31(−3)	5.97(−5)	2.73(−6)	1.25(−7)	5.71(−9)	2.61(−10)	1.19(−11)	5.45(−13)
0.4	1.01(+0)	4.52(−2)	2.07(−3)	9.45(−5)	4.32(−6)	1.98(−7)	9.03(−9)	4.13(−10)	1.89(−11)	8.63(−13)
0.5	1.17(+0)	5.28(−2)	2.41(−3)	1.10(−4)	5.04(−6)	2.30(−7)	1.05(−8)	4.82(−10)	2.20(−11)	1.01(−12)
0.6	1.01(+0)	4.52(−2)	2.07(−3)	9.45(−5)	4.32(−6)	1.98(−7)	9.03(−9)	4.13(−10)	1.89(−11)	8.63(−13)
0.7	6.45(−1)	2.86(−2)	1.31(−3)	5.97(−5)	2.73(−6)	1.25(−7)	5.71(−9)	2.61(−10)	1.19(−11)	5.45(−13)
0.8	3.00(−1)	1.32(−2)	6.01(−4)	2.75(−5)	1.26(−6)	5.75(−8)	2.63(−9)	1.20(−10)	5.49(−12)	2.51(−13)
0.9	9.15(−2)	4.04(−3)	1.85(−4)	8.43(−6)	3.86(−7)	1.76(−8)	8.06(−10)	3.69(−11)	1.71(−12)	9.82(−14)

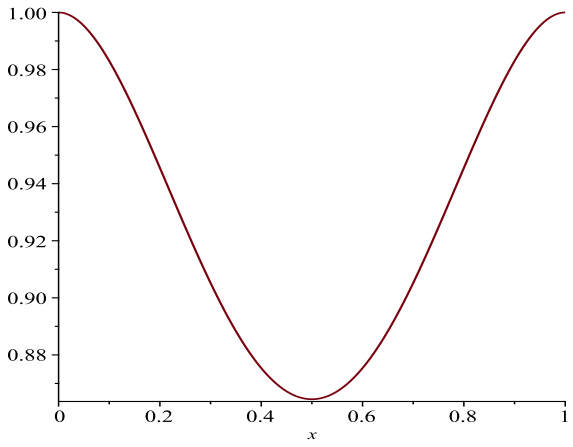

Figure 1. The shape of the nano-actuator evaluated using the fixed point iterative scheme ($\alpha = 20$, $\beta = 5$, $\xi = 4$, $\gamma = 0.325$, $P = 0$, $\kappa = -0.396$, and $\eta = 0.96$).

TABLE 3. Comparison of the value of the maximum deflection of a nano-actuator obtained by other methods versus the proposed scheme ($\alpha = 25$, $\xi = 4$, $\beta = 15$, $\gamma = 0.65$, $P = 0$, $\kappa = 0$, and $\eta = 0$).

Method	Maximum deflection of a nano-actuator
Our proposed PGS	0.135526676798
ADM [30]	0.13486
Numerical [30]	0.13536
Duan–Rach ADM [7]	0.13534

In the second case, we consider a nano-actuator with $\alpha = 25$, $\xi = 4$, $\beta = 0$, $\gamma = 0.65$, and $P = \kappa = \eta = 0$. In Table 4 we report the values of the maximum deflection of the beam. Note that, with 40 iterations, we obtain the maximum deflection accurate to 19 decimal places. In Table 5, we present the residual errors for different iterations, which clearly confirms the high accuracy of the current method and the maximum value of deflection of the beam. The shape of the nano-actuator, evaluated numerically by the proposed approach, is depicted in Figure 2.

TABLE 4. Largest deflection of a nano-actuator whith $\alpha = 25$, $\beta = 0$, $\xi = 4$, $\gamma = 0.65$, $P = 0$, $\kappa = 0$, and $\eta = 0$.

Number of iterations	Maximum deflection of a nano-actuator
$n = 4$	0.088243067359619082527578 1
$n = 8$	0.088780338991896352511286 7
$n = 12$	0.088784540911283703855340 5
$n = 16$	0.088784573830902933433816 3
$n = 20$	0.088784574088812698630071 0
$n = 24$	0.088784574090833300800299 9
$n = 28$	0.088784574090849131271591 4
$n = 32$	0.088784574090849255295916 9
$n = 36$	0.088784574090849256267589 4
$n = 40$	0.088784574090849256275244 2

TABLE 5. Residual errors for the case $\alpha = 25$, $\xi = 4$, $\beta = 0$, $\gamma = 0.65$, $P = 0$, $\kappa = 0$, and $\eta = 0$.

x	$n = 4$	$n = 8$	$n = 12$	$n = 16$	$n = 20$	$n = 24$	$n = 28$	$n = 32$	$n = 36$	$n = 40$
0.1	1.61(−2)	1.25(−4)	9.80(−7)	7.68(-9)	6.01(−11)	4.71(−13)	3.69(−15)	2.89(−17)	2.27(−19)	1.78(−21)
0.2	5.99(−2)	4.67(−4)	3.66(−6)	2.86(-8)	2.24(−10)	1.76(−12)	1.38(−14)	1.08(−16)	8.45(−19)	6.62(−21)
0.3	1.22(−1)	9.52(−4)	7.46(−6)	5.84(-8)	4.58(−10)	3.59(−12)	2.81(−14)	2.20(−16)	1.73(−18)	1.35(−20)
0.4	1.80(−1)	1.41(−3)	1.10(−5)	8.65(-8)	6.77(−10)	5.31(−12)	4.16(−14)	3.26(−16)	2.55(−18)	2.00(−20)
0.5	2.04(−1)	1.60(−3)	1.25(−5)	9.82(-8)	7.69(−10)	6.03(−12)	4.72(−14)	3.70(−16)	2.90(−18)	2.27(−20)
0.6	1.80(−1)	1.41(−3)	1.10(−5)	8.65(-8)	6.77(−10)	5.31(−12)	4.16(−14)	(3.26(−16)	2.55(−18)	2.00(−20)
0.7	1.22(−1)	9.52(−4)	7.46(−6)	5.85(-8)	4.58(−10)	3.59(−12)	2.81(−14)	2.20(−16)	1.73(−18)	1.35(−20)
0.8	5.99(−2)	4.67(−4)	3.66(−6)	2.86(-8)	2.24(−10)	1.76(−12)	1.38(−14)	1.08(−16)	8.45(−19)	6.62(−21)
0.9	1.61(−2)	1.25(−4)	9.80(−7)	7.68(-9)	6.01(−11)	4.71(−13)	3.69(−15)	2.89(−17)	2.27(−19)	1.78(−21)

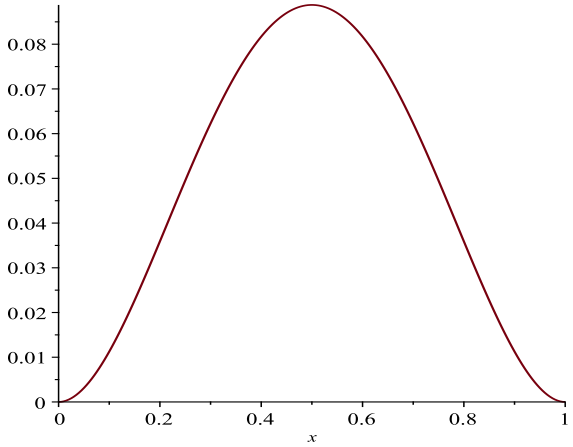

Figure 2. The shape of the nano-actuator is calculated via the fixed point iterative scheme ($\alpha = 25$, $\xi = 4$, $\beta = 0$, $\gamma = 0.65$, and $P = \kappa = \eta = 0$).

In the third case, we consider a nano-actuator with $\alpha = 25$, $\xi = 4$, $\beta = 15$, $\gamma = 0.65$, and $P = \kappa = \eta = 0$. In Table 6 we report the values of the maximum deflection of the beam. Note that, with 42 iterations, we obtain the maximum deflection accurate to 10 decimal places. In Table 7, we report the residual errors for different iterations, which clearly confirms the high accuracy of the current method and the maximum value of deflection of the beam. The shape of the nano-actuator, evaluated numerically by the proposed approach, is depicted in Figure 3.

TABLE 6. largest deflection of a nano-actuator with $\alpha = 25$, $\beta = 15$, $\xi = 4$, $\gamma = 0.65$, and $P = \kappa = \eta = 0$.

Number of iterations	Maximum deflection of a nano-actuator
$n = 6$	0.17006112098767746448693 14
$n = 10$	0.17109913967249769352692 78
$n = 14$	0.17127652554682744787034 79
$n = 18$	0.17129169931285718213259 35
$n = 22$	0.17129299846449236648536 27
$n = 26$	0.17129310970420595722611 58
$n = 30$	0.17129311922915701739609 35
$n = 34$	0.17129312004473574520114 43
$n = 38$	0.17129312011457008758357 36
$n = 42$	0.17129312012054968860794 79

TABLE 7. Residual errors for the case $\alpha = 25$, $\xi = 4$, $\beta = 15$, $\gamma = 0.65$, $P = 0$, $\kappa = 0$, and $\eta = 0$.

x	$n = 6$	$n = 10$	$n = 14$	$n = 18$	$n = 22$	$n = 26$	$n = 30$	$n = 34$	$n = 38$	$n = 42$
0.1	3.32(−2)	2.76(−3)	2.36(−4)	2.02(-5)	1.73(−6)	1.48(−7)	1.27(−8)	1.09(−9)	9.29(−11)	7.96(−12)
0.2	1.37(−1)	1.14(−2)	9.75(−4)	8.35(-5)	7.15(−6)	6.12(−7)	5.24(−8)	4.49(−9)	3.84(−10)	3.29(−11)
0.3	3.14(−1)	2.64(−2)	2.25(−3)	1.93(-4)	1.65(−5)	1.41(−6)	1.21(−7)	1.04(−8)	8.88(−10)	7.60(−11)
0.4	5.12(−1)	4.32(−2)	3.69(−3)	3.16(-4)	2.71(−5)	2.32(−6)	1.98(−7)	1.70(−8)	1.45(−9)	1.25(−10)
0.5	6.03(−1)	5.10(−2)	4.36(−3)	3.74(-4)	3.20(−5)	2.74(−6)	2.34(−7)	2.01(−8)	1.72(−9)	1.47(−10)
0.6	5.12(−1)	4.32(−2)	3.69(−3)	3.16(-4)	2.71(−5)	2.32(−6)	1.98(−7)	1.70(−8)	1.45(−9)	1.25(−10)
0.7	3.14(−1)	2.64(−2)	2.25(−3)	1.93(-4)	1.65(−5)	1.41(−6)	2.81(−7)	1.04(−8)	8.88(−10)	7.60(−11)
0.8	1.37(−1)	1.14(−2)	9.75(−4)	8.35(-5)	7.15(−6)	6.12(−7)	5.24(−8)	4.49(−9)	3.84(−10)	3.29(−11)
0.9	3.32(−2)	2.76(−3)	2.36(−4)	2.02(-5)	1.73(−6)	1.48(−7)	1.27(−8)	1.09(−9)	9.29(−11)	7.96(−12)

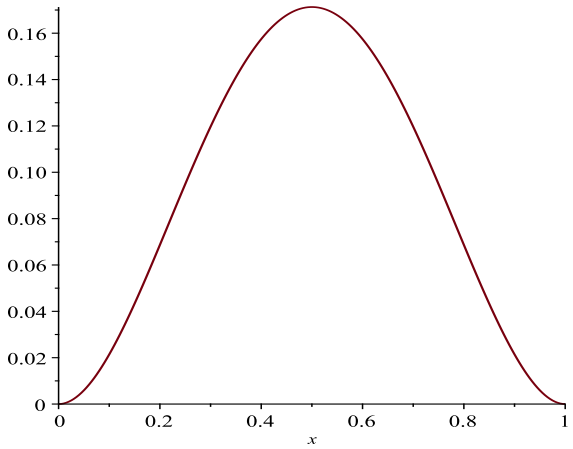

Figure 3. The shape of the nano-actuator evaluated using the fixed point iterative scheme ($\alpha = 25$, $\xi = 4$, $\beta = 15$, $\gamma = 0.65$, $P = 0$, $\kappa = 0$, and $\eta = 0$).

6. CONCLUSION

In this study, a recently developed fixed point iterative scheme, based on Green's functions, has been successfully implemented for the numerical solution of the buckling of a nano-actuator under nonlinear forces. The nano-actuators problem under study is governed by a general type equation that contains integro-differential terms and nonlinear forces. The resulting equation is a nonlinear 4^{th} order integro-differential BVP. The values of the maximum deflection of the beam are obtained with high accuracy and a graph of the nano-actuator is provided for different values of the parameters. Comparison with other numerical methods was conducted and the outcomes confirm that the proposed scheme is highly accurate, robust and converges fast. Finally, our method can be extended to a wide spectrum of integro-differential BVPs.

Funding: Not applicable.

Conflicts of interest/Competing interests: The authors declare that they have no conflict of interest.
Availability of data and material: Not applicable.
Code availability: Not applicable.
Authors' contributions: The authors contributed equally to the work.

References

[1] Abushammala, M., Khuri, S. A. and Sayfy, A. (2015). A novel fixed point iteration method for the solution of third order boundary value problems. *Applied Mathematics and Computation, 271*, 131-141.
[2] Ansari, R., Gholami, R., Faghih Shojaei, M., Mohammadi, V. and Sahmani, S. (2014). Surface stress effect on the pull-in instability of circular nanoplates. *Acta Astronautica, 102*, 140-150.
[3] Bacciocchi, M., Eisenberger, M., Fantuzzi, N., Tornabene, F. and Viola, E. (2016). Vibration analysis of variable thickness plates and shells by the generalized differential quadrature method. *Composite Structures, 156*, 218-237.
[4] Batra, R.C., Porfiri, M. and Spinello, D. (2007). Review of modeling electrostatically actuated microelectromechanical systems. *Smart Materials and Structures 16*, 23-31.
[5] Bougoffa, L., Rach, R., Wazwaz, A.M. and Duan, J. (2014). On the Adomian decomposition method for solving the Stefan problem. *International Journal of Numerical Methods for Heat and Fluid Flow, 25(4)*, 912-928.
[6] Bougoffa, L. and Wazwaz, A.M. (2015). New approximate solutions of the Blasius equation. *International journal of Numerical methods for Heat and Fluid Flow, 25(7)*, 1590-1599.
[7] Ghalambaz, M., Ghalambaz, M. and Edalatifar, M. (2016). A new analytic solution for buckling of doubly clamped nano-actuators with integro differential governing equation using Duan–Rach Adomian decomposition method. *Applied Mathematical Modeling 40(15-16)*, 7293-7302.
[8] Ghalambaz, M., Noghrehabadi, A., Abadyan, M., Beni, Y.T., Abadi, A.N. and Abadi, M.N. (2011). A new power series solution on the electrostatic pull-in instability of nano cantilever actuators. *Procedia Engineering 10*, 3708-3716.
[9] Kafri, H. Q., Khuri, S.A. and Sayfy, A. (2016). A new approach based on embedding Green's functions into fixed-point iterations for highly accurate solution to Troesch's problem. *International Journal for Computational Methods in Engineering Science and Mechanics, 17(2)*, 93-105.
[10] Kafri, H. Q. and Khuri, S.A. (2016). Bratu's problem: A novel approach using fixed-point iterations and Green's functions. *Computer Physics Communications, 198*, 97-104.
[11] Kanani, A.S., Niknam, H., Ohadi, A.R. and Aghdam, M.M. (2014). Effect of nonlinear elastic foundation on large amplitude free and forced vibration of functionally graded beam. *Composite Structures, 115*, 60-68.
[12] Keivani, M., Koochi, A. and Abadyan, M. (2016). New model for stability analysis of electromechanical nano-actuator based on Gurtin–Murdoch and consistent couple-stress theories. *Journal of Vibroengineering, 18(3)*, 1406-1416.
[13] Khuri, S.A. and Sayfy, A. (2014). Variational iteration method: Green's functions

and fixed point iterations perspective. *Applied Mathematics Letters, 32*, 28-34.
[14] Khuri, S.A. and Louhichi, I. (2018). A novel Ishikawa-Green's fixed point scheme for the solution of BVPs. *Applied Mathematics Letters, 82*, 50-57.
[15] Khuri, S.A. and Wazwaz, A.M. (2018). The successive differentiation computer–assisted method for solving well-known scientific and engineering models. *International Journal of Numerical Methods for Heat & Fluid Flow, 28(12),* 2862-2873.
[16] Khuri, S.A. and Wazwaz, A.M. (2013). A variational approach to a BVP arising in the modeling of electrically conducting solids. *Central European Journal of Engineering 3 (1)*, 106-112.
[17] Khuri, S.A. and Sayfy, A. (2015). A novel fixed point scheme: proper setting of variational iteration method for BVPs. *Applied Mathematics Letters, 48*, 75-84.
[18] Koochi, A., Kazemi, A., Khandani, F. and Abadyan, M. (2012). Influence of surface effects on size-dependent instability of nano-actuators in the presence of quantum vacuum fluctuations. *Phys. Scr., 85*, 035804.
[19] Koochi, A., Kazemi, A.S., Beni, Y.T., Yekrangi, A., and Abadyan, M. (2010). Theoretical study of the effect of Casimir attraction on the pull–in behavior of beam–type NEMS using modified Adomian method. *Phys. E Low Dimens. Syst. Nanostruct., 43(2)*, 625-632.
[20] Mohebshahedin, A. and Farrokhabadi, A. (2015). The influence of the surface energy on the instability behavior of NEMS structures in presence of intermolecular attractions. *International Journal of Mechanical Sciences, 101-102*, 437-448.
[21] Noghrehabadi, A., Ghalambaz, M., and Ghanbarzadeha, A. (2012). Buckling of multi wall carbon nanotube cantilevers in the vicinity of graphite sheets using monotone positive method. *Journal of Computational and Applied Research in Mechanical Engineering, 1*, 89-97.
[22] Noghrehabadi, A., Beni, Y.T., Koochi, A., Kazemi, A.S., Yekrangi, A., Abadyan, M. and Abadi, M.N. (2011). Closed-form approximations of the pull-in parameters and stress field of electrostatic cantilevers nano-actuators considering van der Waals attraction. *Procedia Engineering, 10*, 3750-3756.
[23] Noghrehabadi, A., Ghalambaz, M., Beni, Y.T., Abadyan, M., Abadi, M.N.and Abadi, M.N. (2011). A new solution on the buckling and stable length of multi wall carbon nanotube probes near graphite sheets. *Procedia Engineering, 10*, 3725-3733.
[24] Noghrehabadi, A., Ghalambaz, M. and Ghanbarzadeh, A. (2012). A new approach to the electrostatic pull-in instability of nanocantilever actuators using the ADM–Padé technique. *Comput. Math. Appl., 64(9)*, 2806-2815.
[25] Shanab, R.A., Attia, M.A. and Mohamed, S.A. (2017). Nonlinear analysis of functionally graded nanoscale beams incorporating the surface energy and microstructure effects. *International Journal of Mechanical Sciences, 131-132*, 908–923.
[26] Shivanian, E. and and Ansari, M.R. (2019). Buckling of Doubly Clamped Nano-Actuators in General Form through Optimized Chebyshev Polynomials with Interior Point Algorithm. *Acta Physica Polonica, A.* Vol. 135, No. 3.
[27] SoltanRezaee, M., Farrokhabadi, A. and Ghazavi, M.R. (2016). The influence of dispersion forces on the size-dependent pull-in instability of general cantilever nano–beams containing geometrical non-linearity. *International Journal of Mechanical Sciences, 119*, 114-124.

[28] Soroush, R., Koochi, Kazemi, A.S. and Abadyan, M. (2012). Modeling the effect of Van Der Waals attraction on the instability of electrostatic cantilever and doubly-supported nano-beams using modified Adomian method. *Int. J. Struct. Stab. Dyn., 12(5)*, 1250036.
[29] Wazwaz, A.M., Rach, R. and Bougoffa, L. (2016). Dual solutions for nonlinear boundary value problems by the Adomian decomposition method. *International J. of Numerical Methods for Heat and Fluid Flow, 26(8)*, 2393-2409.
[30] Yazdanpanahi, E., Noghrehabadi, A. and Ghalambaz, M. (2014). Pull-in instability of electrostatic doubly clamped nano actuators: introduction of a balanced liquid layer (BLL). *Int. J. Non-Linear Mech., 58*, 128-138.
[31] Younis, M.I., Abdel-Rahman, E.M. and Nayfeh, A. (2003). A reduced-order model for electrically actuated microbeam-based MEMS. *Journal of Microelectromechanical Systems, 12(5)*, 672-680.

[1]Department of Mathematics & Statistics, College of Arts & Sciences, American University of Sharjah, P.O.Box 26666, Sharjah , United Arab Emirates.
Email address: afyousef@aus.edu

[2]Department of Mathematics. The University of Jordan. Amman 11942. Jordan.
Email address: abd.yousef@ju.edu.jo

[2]Department of Mathematics & Statistics, College of Arts & Sciences, American University of Sharjah, P.O.Box 26666, Sharjah , United Arab Emirates.
Email address: skhoury@aus.edu

[3]Department of Mathematics & Statistics, College of Arts & Sciences, American University of Sharjah, P.O.Box 26666, Sharjah , United Arab Emirates.

*Corresponding author
Email address: ilouhichi@aus.edu